JOURNAL OF THERMOPHYSICS AND HEAT TRANSFER
Vol. 26, No. 4, October–December 2012

Influence of Turbulent Fluctuations on the Radiation Intensity Emitted from Exhaust Plumes

David L. Blunck,* Matthew E. Harvazinski,† Charles L. Merkle,‡ and Jay P. Gore§
Purdue University, West Lafayette, Indiana 47907

DOI: 10.2514/1.T3802

Measured and computed mean and fluctuating radiation intensities are reported for a subsonic exhaust plume and used to characterize the influence of turbulent fluctuations on mean radiation properties. Narrowband radiation intensity measurements were acquired using an infrared camera fitted with a narrowband filter (4.34 ± 0.1 μm). Unsteady three-dimensional calculations were used to estimate both time-dependent and mean temperature and partial pressure values of the exhaust species in the flow. From these scalar values the mean and root mean square of the radiation intensity were calculated using a narrowband radiation model. Axial distributions of the calculated intensities based on the time-dependent quantities show trends similar to those measured, but consistently overpredict the intensity by 40%. Intensity distributions based on mean scalars were in better quantitative agreement, but decay more rapidly downstream than experimental data. Turbulent fluctuations have little effect on the mean radiation intensity near the nozzle exit, but they become increasingly more important downstream in the flow. The influence of turbulent fluctuations on mean intensity values increases with radial distance from the centerline. This trend correlates to increases in normalized fluctuations in the temperature and radiation intensity.

Nomenclature

CO_2	=	carbon dioxide
D	=	exit diameter of nozzle, cm
I_λ	=	spectral intensity, W/m^2-sr-μm
M	=	Mach number
r	=	radial distance from nozzle, cm
T	=	temperature, K
$\bar{T}$	=	mean temperature, K
t	=	time, s
X	=	mole fraction
z	=	axial distance from the nozzle exit, cm
α_λ	=	spectral absorption and response of optics and detector, μm^{-1}
λ_1	=	minimum wavelength transmitted through filter, μm
λ_2	=	maximum wavelength transmitted through filter, μm
Φ	=	equivalence ratio

Subscripts

$\Delta\lambda$	=	integrated between λ_1 and λ_2
max	=	maximum value
mean	=	mean value
stdev	=	standard deviation
rms	=	root mean square

Presented as Paper 2010-238 at the 48th AIAA Aerospace Sciences Meeting, Orlando, Florida, 4–7 January 2010; received 12 August 2011; revision received 24 May 2012; accepted for publication 26 May 2012.

*Currently, Mechanical Engineer, Combustion Branch in the Propulsion Directorate, AFRL/RZTC Building 490, 1950 Fifth Street, Wright–Patterson Air Force Base, Ohio 45433. Member AIAA.

†Graduate Research Assistant, School of Mechanical Engineering, 585 Purdue Mall. Member AIAA.

‡Former Reilly Professor of Engineering, School of Mechanical Engineering, 585 Purdue Mall. Fellow AIAA.

§Reilly Professor of Combustion, School of Mechanical Engineering and Director of the Energy Center, 500 Central Drive. Fellow AIAA.

I. Introduction

MODELING and measurements of infrared radiation emissions from exhaust plumes are of interest for aircraft security [1] and for understanding scalar distribution in high-temperature flows. Modeling of radiation emissions from exhaust plumes [2–7] is important for developing safety guidelines. Measurements of the radiation intensity provide nonintrusive information regarding changes in the scalar distribution and turbulent nature of the jets [8,9]. Comparisons of measured and computed mean and fluctuating radiation intensities provide insights into the validity of scalar calculations.

The plume core is a major contributor to the radiation emitted from exhaust streams [5]. In the core the high-temperature and species concentrations of the exhaust are maintained because little entrainment and mixing occurs [6]. Techniques to reduce radiation emissions from exhaust flows are often analyzed with respect to changes in the length and size of the core [6,10,11]. Heragu et al. [3] and Decher [6] used models of cores to estimate changes in the radiation intensity and radiant power emitted by plumes for different flow conditions.

Coupling can occur between radiation heat transfer and fluctuations in the temperature and species concentrations in turbulent flows. Radiation losses influence fluctuations in the fluid by altering the temperature and subsequently the density within the flow. Conversely, fluctuations in the temperature and radiating species affect the radiation emitted, absorbed, and scattered within the flow [12]. The interdependence of these two phenomena is known as turbulence radiation interactions [13–17]. This work focuses on the effect of scalar fluctuations on the radiation intensity emitted from subsonic plumes. Relevant flame literature is now briefly summarized, followed by a review of nonreacting flow literature.

Jeng et al. [18] developed a stochastic method [19–21] to account for fluctuations in the temperature and species concentrations in turbulent flames. A time-averaged probably density function of the mixture fraction was randomly sampled and used to predict scalar values and then calculate the spectral intensity. The calculated spectral intensity was averaged until a converged solution was obtained. These values, and predictions using mean scalar values, were compared with measurements along diametric paths. The stochastic technique overpredicted the spectral intensity on the order of 10–30% for radiation emitted from carbon dioxide [18]. Gore et al. [22,23] studied the importance of turbulent fluctuations in carbon monoxide and hydrogen flames using the same approach. In the carbon monoxide flames, only a 10% deviation was noted

between the spectral intensity found by accounting for and neglecting scalar fluctuations [22]. In the hydrogen flames, the stochastic predictions were as much as twice as large as those using mean scalar values [23], and had better agreement with measured values.

Zheng et al. [24,25] reported turbulent radiation statistics for jet flames and found that the effect of turbulent fluctuations on mean intensity values varies spatially. For diametric paths (i.e., through the centerline) the calculated spectral intensity using mean scalar values for methane flames diluted with nitrogen typically had good agreement with measured values. For chordlike paths (i.e., away from centerline) calculations found using mean scalar properties underpredicted the spectral intensity by as much as 50%. The greater influence of turbulent fluctuations for chordlike paths was attributed to larger fluctuations [25].

Pearce and Varma [26] reported in a reacting plume that the effects of turbulent fluctuations on mean radiation properties vary spatially. Line-by-line calculations of the radiation intensity were performed using temperature and carbon dioxide concentrations calculated using a two-dimensional reacting flow model. Augmentation of the radiation intensity due to turbulent fluctuations was minimal along the plume axis, but became more significant for chordlike paths (up to a factor of 2.5). The authors suggested that the influence of turbulent fluctuations will be greater in the regions of a plume where few chemical reactions occur [26].

Gupta et al. [27] and Mazumder and Modest [28] calculated the effect of turbulent fluctuations on radiative heat loss and scalar values in nonreacting channel [27] and bluff-body [28] flows. In the channel flow, turbulent fluctuations had a minimal effect on the radiation emitted by the flow due to small temperature fluctuations (3% of mean scalar value) [27]. In the bluff-body flow, turbulent fluctuations increased the radiant heat flux to the wall by 5% for flow conditions when the exhaust was 200 K higher than the surrounding air [28].

Given this review of the relevant literature and the importance of accurate modeling of exhaust plumes, the objectives of this work are as follows:

1) Measure and predict the mean and root mean square of the radiation intensity emitted from exhaust plumes at varying axial and radial locations.

2) Determine the influence of turbulent fluctuations on the radiation intensity emitted from exhaust plumes.

Findings from this study can be used for guidance in determining when turbulent fluctuations should be considered for modeling the radiation emitted from exhaust plumes.

II. Experimental Arrangement

A. Plume Generation

The experimental arrangement has been reported previously [8] and is summarized and illustrated in Fig. 1. A single combustor can mounted in a pressure vessel was used to generate the hot exhaust products. Jet A fuel was injected into the combustor, where it mixed with dry air and burned. Fuel flow rates were measured using a calibrated turbine flow meter. Air flow rates were determined by measuring the pressure and temperature upstream of a choked orifice.

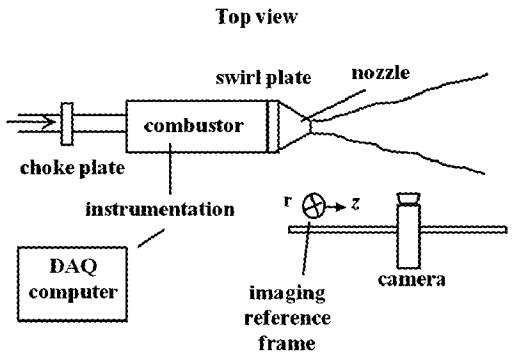

Fig. 1 Experimental arrangement for generating plume and obtaining radiation intensity measurements.

A portion of the air was used for convective cooling of the combustor liner. Consequently, what is reported is a global equivalence ratio. Comparison between chemical equilibrium calculations and species measurements upstream of the nozzle [8] indicate that the flow is nonreacting at the nozzle exit. A plate with holes drilled at approximately 10 deg was placed between the combustor and the nozzle to pressurize the system and impart swirl to the flow.

A subsonic axisymmetric nozzle with an exit diameter of 9.1 cm was used for testing. The temperature at the nozzle exit (925 K) was found using isentropic relationships and the temperature measured within the nozzle. The Mach and Reynolds numbers at the nozzle exit were determined based on the measured temperature and air mass flow rate [9]. A layer of insulation (9 cm) was applied to the nozzle to reduce heat loss from the flow.

Measurements were acquired for an exhaust plume with an air flow rate of 0.65 kg/s and a fuel flow rate of 11 g/s. These conditions correspond to an equivalence ratio of 0.25, a Mach number equal to 0.4, and a Reynolds number of 2.3×10^5. The carbon dioxide and water vapor mole fractions were 0.036 and 0.034, respectively, based on chemical equilibrium calculations. These conditions were used to specify the computational boundary conditions.

B. Radiation Measurements

A FLIR Phoenix infrared camera was used to obtain spectrally integrated radiation intensity measurements:

$$I_{\Delta\lambda} = \int_{\lambda_1}^{\lambda_2} \alpha_\lambda I_\lambda \, \mathrm{d}\lambda \tag{1}$$

α_λ accounts for variations in the spectral response of the detector and losses through camera optics and was obtained from the camera and filter manufacturers. The integration limits represent the spectral range allowed through the camera optics and filter. The spectrally integrated intensity is that incident on the detector. The camera was traversed parallel to the axis of the plume, as illustrated in Fig. 1. The axial location is the distance from the nozzle exit and the radial location is the orthogonal distance from the plume centerline as viewed by the camera. A 4.34 ± 0.1 μm narrowband filter was used to isolate radiation from carbon dioxide and improve the characterization of the spectral response of the detector. Self-absorption of emission from the plume within the spectral range of the filter was included in the calculations. Measurements acquired without the filter were comparable to those with the filter, indicating that radiation emitted from soot and water vapor is negligible. Calculations showed that approximately 40% or more of emissions from the plume are transmitted through the atmosphere. Calibrations were performed by measuring the radiation intensity emitted from a blackbody at known temperatures. The blackbody was placed the same distance from the camera as the plume centerline, which is an approximate technique for compensating for the atmospheric attenuation of the radiation intensity during testing. One limitation of this approach is that atmospheric carbon dioxide concentrations would be slightly higher at the time of testing than when the calibration was performed as a result of the combustion products exhausting into the air. A second limitation is that the blackbody emits continuously across spectrum whereas the plume emits at discrete lines.

The integration time of the camera was set to 0.05 ms. Seven thousand consecutive measurements were obtained and used for processing. The spatial resolution of each pixel on the detector was approximately 0.03 cm^2. Centerline intensity values are reported for axial distances greater than 2 cm away from the nozzle exit ($z/D > 0.25$) to avoid reporting radiation emitted from the nozzle and the surrounding insulation. The average uncertainty in the measurements is 30% (95% confidence) for intensity values greater than 20% of the peak value and 100% for intensity values less than 20% of the peak [8]. This is based on repeated measurements of an auxiliary experiment and a Chi-squared distribution. Uncertainty bars are reported in the relevant figures. During the auxiliary experiment repeated measurements were made using the same arrangement but with at different operating conditions.

III. Computational Methods

A. Flowfield Calculations

A three-dimensional time-dependent computational fluid dynamics calculation of the coupled Navier–Stokes equations were used to predict the velocity, pressure, temperature, and density fields within the nozzle and the plume. The computational domain begins at the nozzle inlet and extends axially 18 diameters downstream (1.6 m) from the nozzle exit and 9 diameters (0.8 m) away from the centerline in the radial direction as shown in Fig. 2. Grid stretching was used in the axial and radial directions away from the region of interest to prevent the reflection of disturbances from the far-field boundaries. The grid used contained approximately 2.4 million grid points. The working fluid was simulated as a mixture of four fluids: carbon dioxide, nitrogen, oxygen, and water vapor; each treated as a distinct inert species. Properties for the water vapor came from the NIST REFPROP database [29]. Properties of the other species were determined using an ideal gas equation of state and a Sutherland model for the viscosity. The governing equations were solved using a finite volume algorithm that was second-order-accurate in both time and space [30,31]. A physical time step of 1 μs was used and a well-converged solution was obtained using ten inner iterations per time step. All calculations were performed using detached eddy simulation [32–35] with the two-equation k-ω model used for the subgrid scale turbulence and near-wall region [36]. The detached eddy calculations resolve the large-scale eddies where the grid and time-scales provide sufficient resolution while Reynolds-averaged Navier–Stokes calculations model the turbulence at the smaller time and length scales. In the present case large-scale vortices shed from the nozzle are directly computed.

The measured stagnation pressure and temperature, calculated species mass fractions, and swirl angle were used as boundary conditions at the nozzle inlet. The swirl angle was specified based on the angle at which holes in the back pressure plate were drilled (~10 deg). A wall boundary was used to represent the insulation surrounding the nozzle. Atmospheric pressure, temperature, and mass fractions were prescribed at the far-field boundaries. Adiabatic no-slip boundary conditions were applied at the walls. The initial condition for the fluid both inside and outside the nozzle was taken to be quiescent at atmospheric temperature and pressure. When the calculations were initialized ($t = 0$) a diaphragm was broken at the upstream end of the domain so that the heated fluid in the jet began to traverse first through the nozzle and then the external portion of the computational domain. Calculations were run for 20 ms before scalar values were collected to guarantee that the jet had propagated to the downstream end of the domain and to ensure that the initial transient had propagated out of the domain. The standard deviation of the mean values from 10 sets of 60 calculations of carbon dioxide mole fractions and temperature normalized by mean values are reported in Table 1 as an indication of the variation in the calculations.

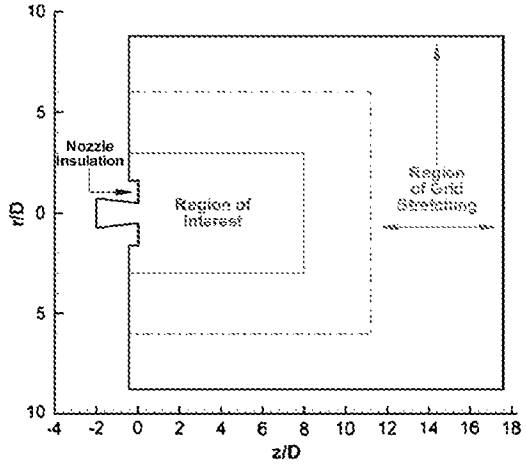

Fig. 2 Computational domain illustrating the area of interest and the region of grid stretching.

Table 1 Standard deviation of the mean values from 10 sets of 60 calculations of carbon dioxide mole fractions and temperature normalized by mean values along the centerline

z/D	$X_{CO_2 stdev}/X_{CO_2 mean}$	T_{stdev}/T_{mean}
0.00	0.00	0.00
0.22	0.00	0.00
0.44	0.00	0.00
0.67	0.00	0.00
0.89	0.00	0.00
1.11	0.00	0.00
1.33	0.00	0.00
1.56	0.00	0.00
1.78	0.00	0.00
2.00	0.00	0.00
2.22	0.00	0.00
2.44	0.01	0.01
2.67	0.04	0.03
2.89	0.07	0.05
3.11	0.10	0.06

The radiation intensity and fluid dynamics computations were uncoupled. The time-resolved fluid flowfield was computed ignoring the effect of radiation losses, and pertinent scalar values were stored for postprocessing to obtain the radiation intensity. This postprocessing step is described in the next section. A set of calculations performed considering radiation losses using a Planck mean absorption model indicated a less than a 5 K reduction in the plume temperature.

Representative contour plots of the time-dependent and time-averaged temperature are shown in Figs. 3–5 to demonstrate the nature of the calculated flowfield. The time-dependent temperature contours show the presence of vortices along the periphery of the jet

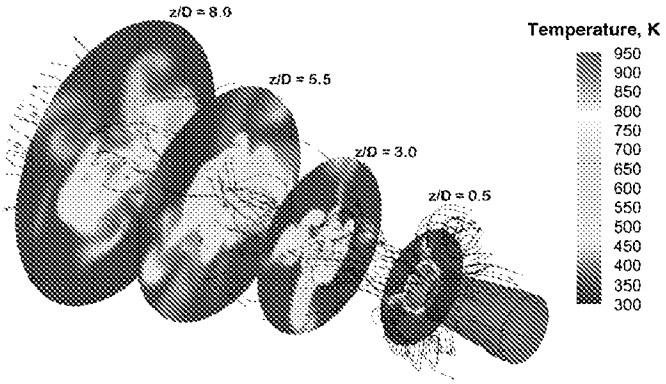

Fig. 3 Time-dependent temperature contour and velocity streamlines of calculations found using a three-dimensional geometry 90 ms from the start of calculations.

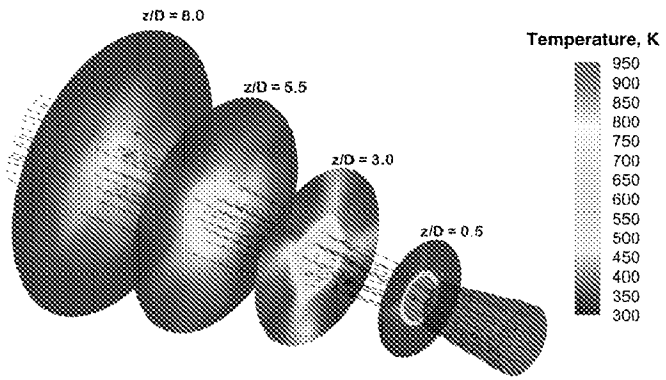

Fig. 4 Time-averaged temperature contour and velocity streamlines of calculations found using three-dimensional geometry 90 ms after the start of calculations.

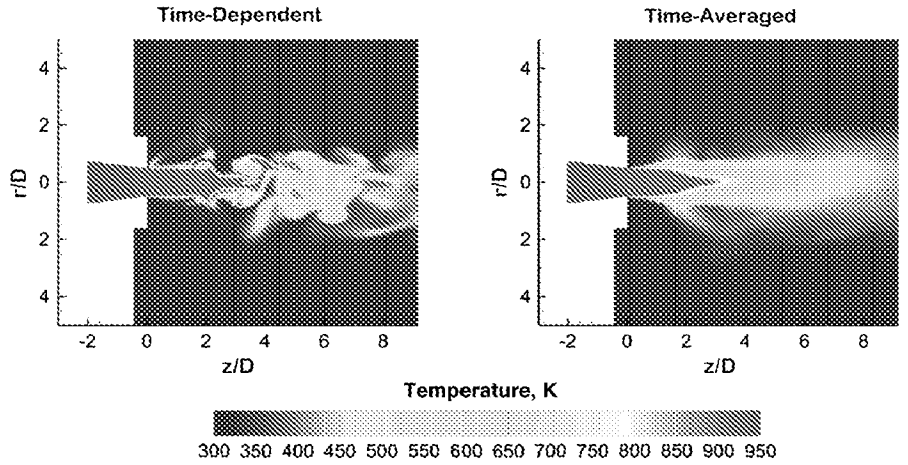

Fig. 5 Time-averaged and time-dependent temperature contours found using three-dimensional geometry 90 ms after the start of calculations; shown is a single slice through the domain.

as it emerges from the nozzle. A well-developed ring vortex is visible in the streamlines just before the $z/D = 0.5$ slice. It is important to note that the ring vortex that forms at the nozzle exit is weak and breaks down as it moves downstream. This structure does not create a recirculation zone near the insulation wall, a clear difference from the two-dimensional calculations. The two-dimensional calculations are reported in the Appendix. The jet-spreading rate is visible in the time-averaged temperature plot.

Two-dimensional calculations were performed using the boundary conditions and numerical schemes just described and are reported in the Appendix. These calculations provided guidance for the three-dimensional calculations and insights into the ability to use two-dimensional scalar calculations to capture the physics of radiation emission from the exhaust flows. Computations were performed for both axisymmetric and Cartesian geometries. In the former case, the calculated scalar values were mirrored around the centerline for radiation intensity calculations. For the Cartesian case, both upper and lower halves of the domain were computed. No swirl was specified at the inlet for the Cartesian case.

B. Radiation Intensity Calculations

The radiation intensity along paths through the plume was determined by solving the radiation transfer equation [37] and Eq. (1) using the mean and time-dependent temperature, water vapor, and carbon dioxide mole fractions. Radiation emission from soot was neglected which was determined to be insignificant based on camera measurements. Paths through (diametric) and off-center from (chordlike) the plume centerline were defined at varying axial locations downstream. Each path through the plume was divided into 500 or more sections.

The procedure for calculating the average of the time-dependent spectrally integrated intensity is as follows: 1) solve the radiation transfer equation using RADCAL [38], a narrowband radiation transfer model, to determine the spectral intensity using the time-dependent scalar values, 2) apply the spectral absorption coefficient to the calculated spectral intensity to allow for comparisons with experimental data, 3) integrate over the spectra to determine the intensity, and 4) update the average intensity.

This procedure was repeated for approximately 650 samples. Scalar values from every 0.01 ms were used. Statistics found using half the sample size agreed with the reported values typically within 10%. The radiation intensity based on the mean quantities was found using the same procedure (i.e., steps 1–3) and the time-averaged scalar values.

The calculated intensities were sensitive to the path orientation through the plume. This is attributed to the finite time over which calculations were performed. To account for the angular variations in the scalar distributions at a fixed axial location, the mean and the normalized root mean square intensity calculations were repeated for thirty diametric paths separated by 12 deg. The average values of these thirty mean and root mean square radiation intensities are reported as representative. The standard deviations of the mean and root mean square intensities for the different orientations were typically within fifteen percent of the mean value. Note that the root mean square and standard deviation are equivalent mathematically in the turbulence literature [39]. The former term is used to describe turbulent fluctuations and the latter term is used in this work as an indication of uncertainty.

IV. Results and Discussion

Figure 6 reports the measured and calculated mean (bottom panel) and normalized mean (top panel) of the radiation intensity emitted along lines of sight through the plume centerline. The intensity reported in the top panel is normalized by the maximum intensity for the respective calculations or measurements to allow trends in the

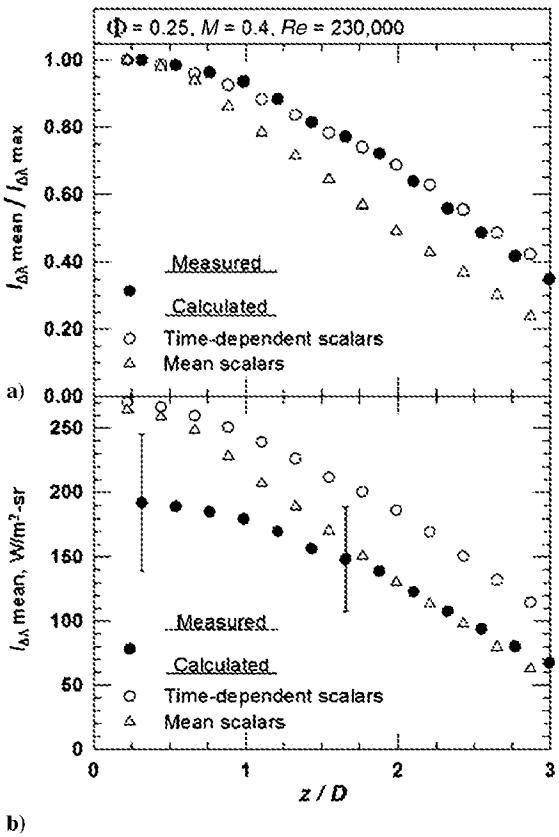

Fig. 6 Measured and calculated normalized (top) and mean (bottom) radiation intensities for lines-of-sight through the plume centerline.

axial variation to be evident. The average calculated radiation intensity is reported for the two methods used. In the one, the radiation is computed from the time-dependent flowfield and then time-averaged (noted as time-dependent scalars). In the other, the flowfield is time-averaged, and the radiation intensity is computed directly from these scalar values (noted as mean scalar). The time-dependent calculations overpredict the intensity on average by 45%, but capture the axial variation in the intensity. The normalized intensity profiles agree within 10%. This suggests that the axial distributions of entrainment and mixing are captured reasonably well in the time-dependent computations. Calculations using mean scalar values typically agree with the measurements (within experimental uncertainty) beyond 1 diameter downstream. The measured trends are not as well captured in the mean scalar calculations as the time-dependent calculations. The normalized intensities under-predict the intensity by up to 40%. The overprediction of the radiation intensity using both computational approaches is attributed to differences between the physical and calculated scalar distributions within the flow. The sensitivity of the intensity calculations to deviations in the scalar distribution is evident in the Cartesian and axisymmetric calculations reported in the Appendix. Uncertainties in the narrow-band radiation model and discrepancies between the camera and modeled total absorption coefficient are additional sources of error.

The radiation intensities calculated using the time-dependent and average scalar values agree within 5% near the nozzle exit. The discrepancy between the computed values increases monotonically downstream until the time-dependent calculations are nearly a factor of two larger than the mean scalar calculations near 3 diameters downstream. Figure 7 shows the axial distribution of the root mean square of the temperature and carbon dioxide mole fractions normalized by mean values. The core region is evident until approximately two diameters downstream, as indicated by steady scalar values. Downstream of the core, the relative fluctuations of the scalar values increase. The calculated $\bar{T}^4/\bar{T}^4$ along the centerline is near unity in the core region and increases to near 1.5 at 4.5 diameters downstream. These findings suggest that turbulent fluctuations have a strong influence on mean radiation properties downstream in the plume. This is in agreement with Pearce and Varma [26] who reported that for a reacting plume, turbulent radiation interactions are more significant toward the edges of the flow.

The larger discrepancy between the time-dependent and mean scalar calculations downstream in the plume correlates to larger normalized fluctuations in the radiation intensity, as shown Fig. 8. Normalized fluctuations in the radiation intensity increase monotonically from 0.01 at 0.5 diameter downstream to 0.4 near 3 diameters downstream. Reasonable agreement between the measured and calculated normalized root mean square of the radiation intensity is observed in this region. Downstream of 3 diameters, fluctuations in the intensity are overpredicted, indicating a discrepancy between the

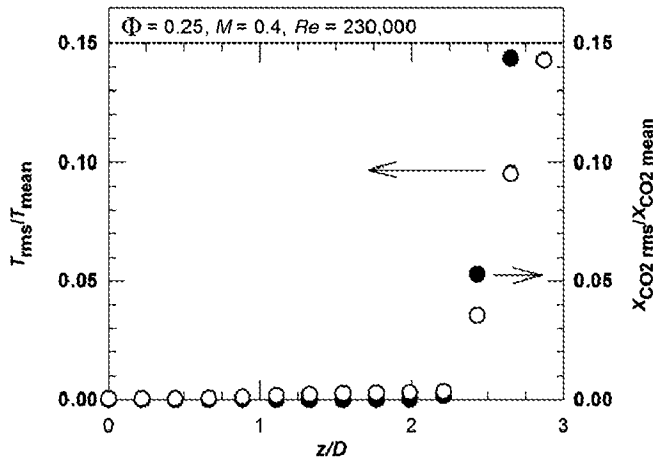

Fig. 7 Axial distribution of the root mean square of the calculated temperature and carbon dioxide mole fractions normalized by the mean value.

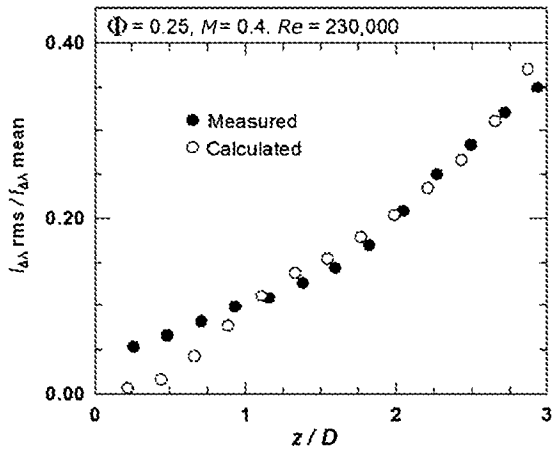

Fig. 8 Measured and calculated normalized root mean squares of the radiation intensity for lines-of-sight through the plume centerline.

modeled and physical flow development. Consequently, calculations (average or fluctuating intensity) beyond 3 diameters downstream are not reported. Kounalakis et al. [40] reported that normalized fluctuations in the spectral intensity emitted from a turbulent hydrogen flame increased monotically from 26 to 107% between 50 and 130 burner diameters downstream, providing evidence of turbulent radiation interactions in the flame. The more rapid development (spatially) of fluctuations in the intensity in exhaust plumes is not surprising considering that scalar values reduce more rapidly in plumes due to entrainment and mixing, whereas in flames, high scalar values are maintained in the flame sheet [9]. In addition, the intensity is more sensitive to changes in the temperature at lower temperatures (e.g., nonreacting plumes) based on Planck's law.

Figure 9 reports the calculated and measured radiation intensities for chordlike paths at axial locations corresponding to 0.5 and 2.5 diameters downstream. Similar to centerline values, the computations capture trends in the measurements and tend to overpredict

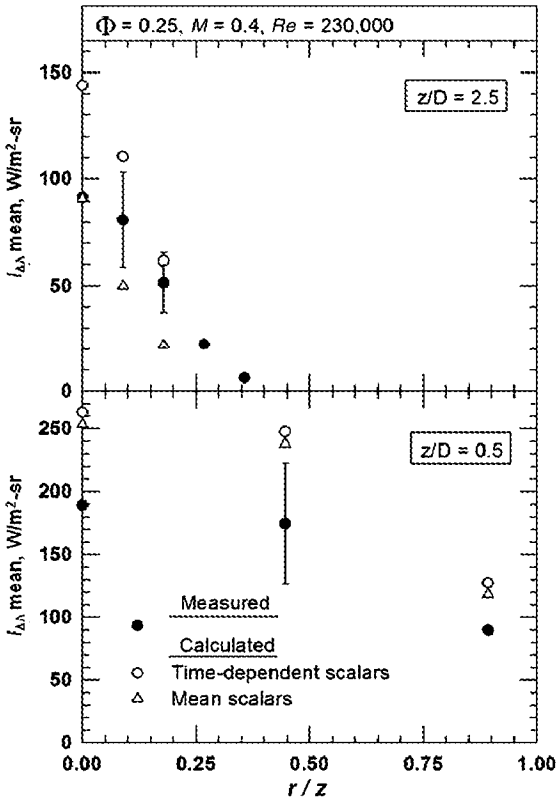

Fig. 9 Measured and calculated mean radiation intensities at axial locations corresponding to half and two and one-half nozzle diameters downstream.

the intensity. At 0.5 diameters downstream, the intensities calculated using time-dependent and mean scalar values agree within 10%. The steady nature of the radiation emitted from the core region minimizes the influence of turbulent fluctuations. At 2.5 diameters downstream calculations using time-dependent scalars overpredict the intensity relative to the mean scalar calculations by a factor of 1.5 near the centerline. The discrepancy in the computations increases monotonically with radial distance until time-dependent calculations are larger than the time-averaged calculations by a factor of nearly 3 (near $r/z = 0.18$). The influence of turbulent fluctuations increases toward the edges of the plume as a result of larger fluctuations in scalar values and an increased sensitivity of the intensity to fluctuations at lower temperatures. Figure 10 shows the calculated root mean square of the temperature and carbon dioxide mole fractions normalized by the mean value at axial locations corresponding to 0.5 and 2.5 nozzle diameters downstream. At 0.5 diameter downstream, scalar values are constant near the centerline and fluctuate in the shear layer surrounding the core (e.g., $r/z = 0.9$), Fluctuations of scalar values in the shear layer cause the fluctuations of the radiation intensity observed for lines of sight through the core region (e.g., $0 < z/D < 2$ in Fig. 8). At 2.5 diameters downstream relative fluctuations in temperature and carbon dioxide mole fractions increase with distance from the centerline until reaching the edges of the plume and are an order of magnitude larger than the values at 0.5 diameters downstream. The increase in the relative fluctuation of carbon dioxide concentration observed for $r/z > 0.45$ at 2.5 diameters downstream is due to the mean mole fraction tending toward 0. The increase in scalar fluctuations toward the edges of the plume is caused by the scalar values fluctuating between the hot exhaust products and cold surrounding air. Zheng et al. [25] found that turbulent fluctuations have a larger effect on mean properties away from the centerline for turbulent methane/hydrogen/nitrogen flames. This trend was correlated to an increase in normalized temperature fluctuations toward the edges of the flame.

Figure 11 reports the calculated and measured normalized root mean squares of the radiation intensity for chordlike paths

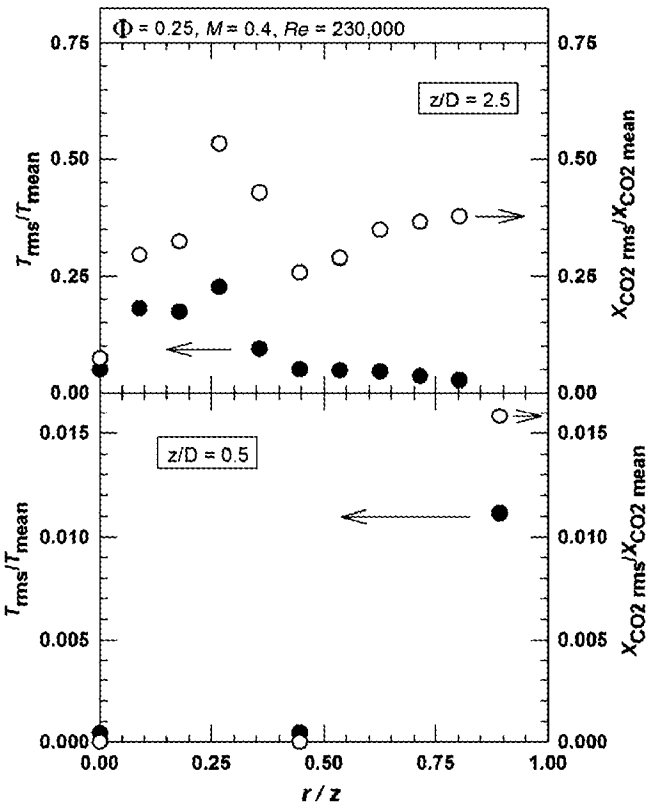

Fig. 10 Calculated root mean square of the temperature and carbon dioxide mole fractions normalized by the mean value at axial locations corresponding to 0.5 and 2.5 diameters downstream.

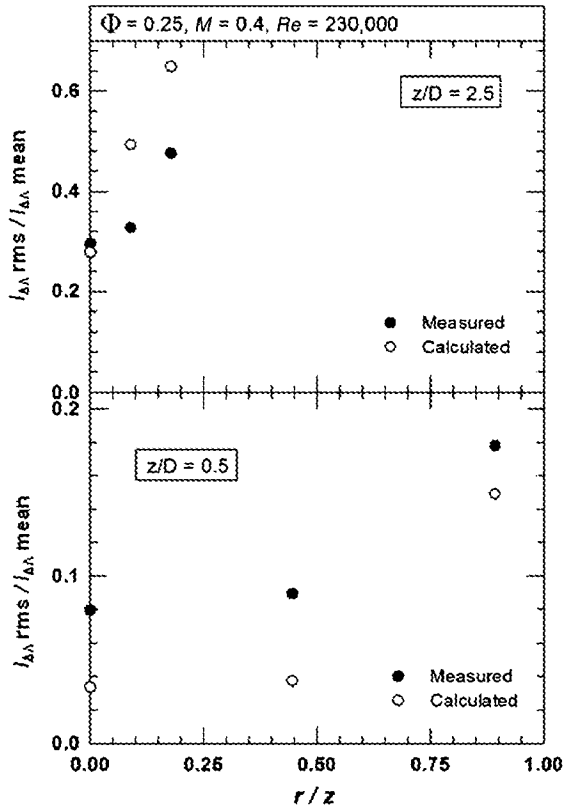

Fig. 11 Measured and calculated normalized root mean squares of the radiation intensity at axial locations corresponding to 0.5 and 2.5 nozzle diameters downstream.

corresponding to axial locations at 0.5 and 2.5 diameters downstream. Normalized fluctuations in calculated and measured radiation intensity increase radially, in agreement with trends reported at other axial locations [9] and for turbulent flames [26,41]. Fluctuations in the scalar values toward the edges of the flow increase the relative fluctuations in the radiation intensity.

V. Conclusions

The radiation intensity emitted from a subsonic exhaust plume was calculated using mean and time-dependent scalar values using three-dimensional geometries. For the operating conditions and nozzle geometry studied the specific conclusions of this work are as follows:

1) Turbulent fluctuations have little effect on the mean radiation intensity near the nozzle exit but become increasingly more important downstream in the flow.

2) The influence of turbulent fluctuations on mean intensity values increases with radial distance from the centerline. This trend correlates to increases in normalized fluctuations in the temperature and radiation intensity.

Appendix

Two-dimensional calculations are reported and compared with three-dimensional calculations. For the conditions studied, three-dimensional calculations were required to correctly capture trends in the mean and root mean square of the radiation intensity emitted downstream of the core region. Figure A1 reports the calculated centerline intensity based on time-dependent and mean scalar calculations for axisymmetric and Cartesian geometries. The axisymmetric calculations (top panel) using both time-dependent and mean scalar values tend to under-predict the intensity near the nozzle exit and overpredict the intensity downstream. The decay in the calculated intensity between 2 and 3.5 diameters downstream is an average of 35%, nearly half of that for the measurements. In the Cartesian geometry case (i.e., slice through plume), trends in the calculations using mean scalars are nearly identical to that for the

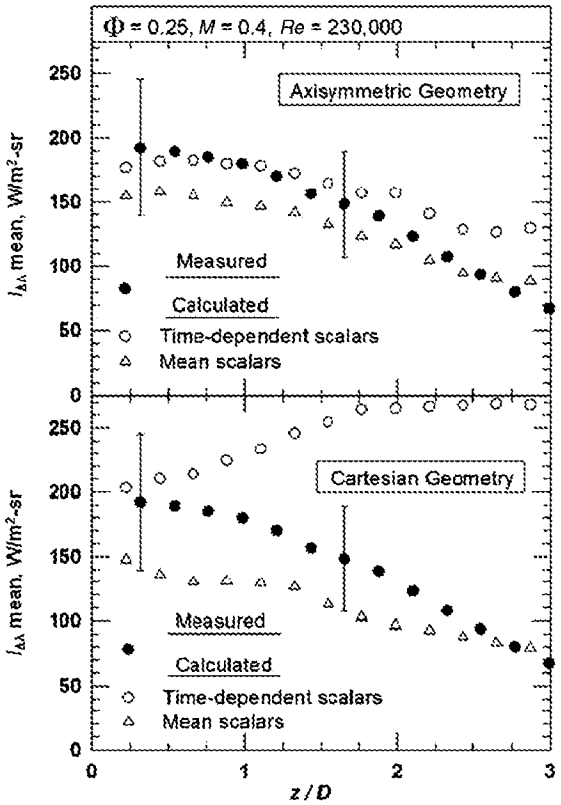

Fig. A1 Measured and calculated radiation intensities along the plume centerline using scalar values found from Cartesian (bottom) and axisymmetric (top) two-dimensional calculations.

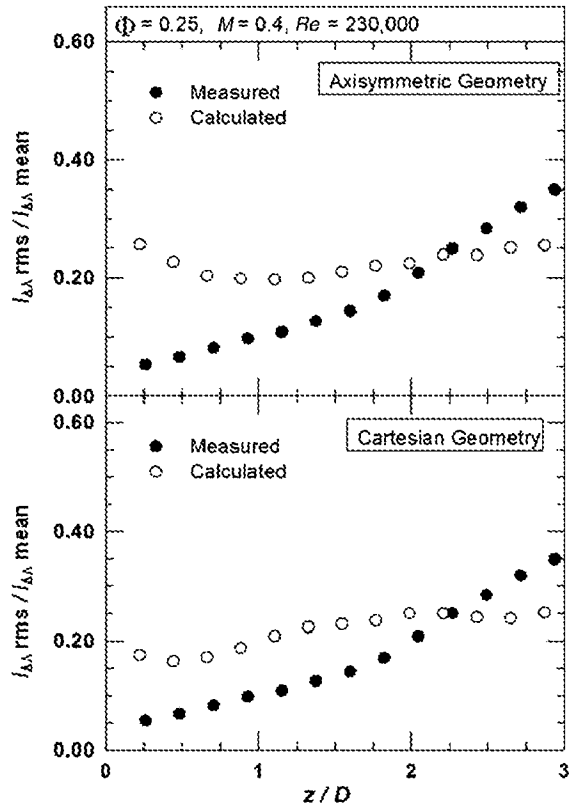

Fig. A2 Measured and calculated normalized root mean squares of the radiation intensity along the centerline using scalar values found from Cartesian (bottom) and axisymmetric (top) two-dimensional calculations.

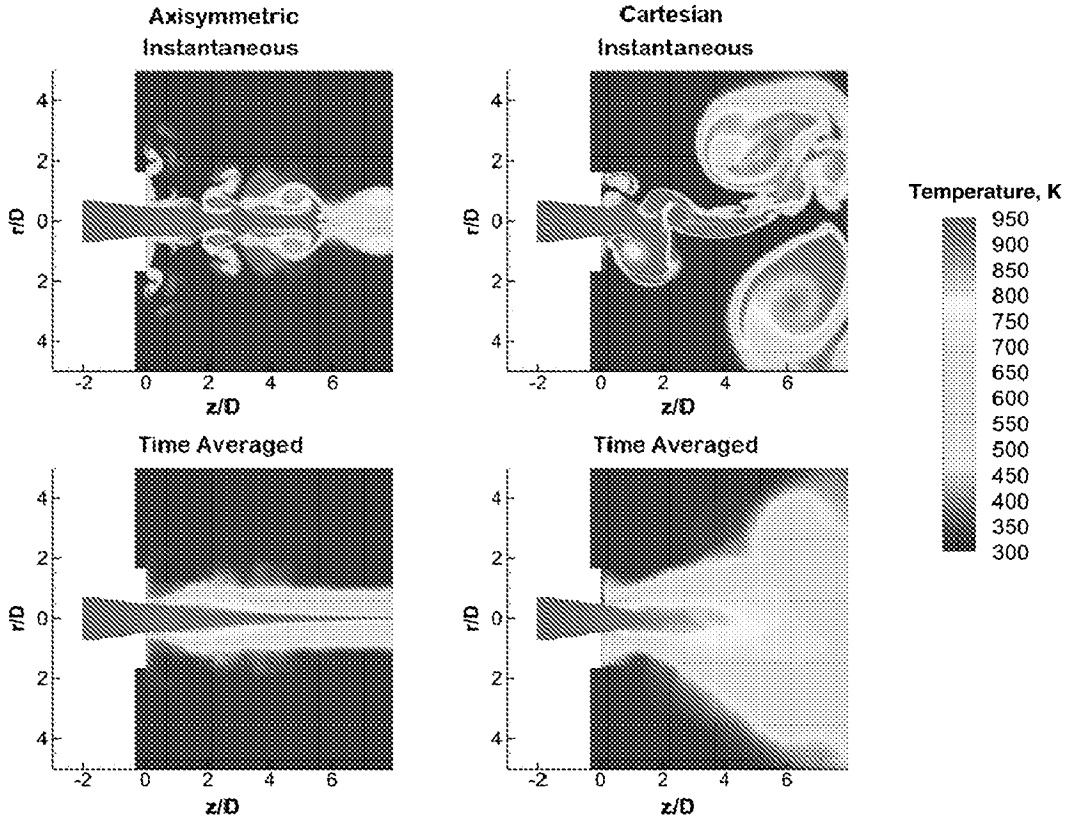

Fig. A3 Time-dependent and average temperature profiles calculated using axisymmetric (left) and Cartesian (right) geometries after 90 ms.

axisymmetric case. The computations using time-dependent scalars increase between the nozzle exit and 2 diameters downstream, before plateauing between 2 and 3 diameters downstream, and then decaying beyond 3 diameters downstream. This surprising trend is caused by the expansion of large vortical structures in the flow, as is discussed shortly. The calculated and measured normalized root mean squares of the radiation intensities are reported in Fig. A2. In both the axisymmetric and Cartesian cases, the fluctuations are overpredicted near the nozzle and underpredicted downstream of the core.

Figure A3 illustrates the time-dependent and time-averaged temperature profiles for the axisymmetric and Cartesian geometry calculations. In both sets of the two-dimensional calculations, a recirculation zone forms near the large back-step region formed by the insulation at the nozzle exit. This is evident in the time-dependent images. These recirculation zones were not evident in the time-dependent three-dimensional calculations or the infrared images acquired using the infrared camera. In the three-dimensional calculations, small ring vortices form close to the nozzle. These vortices break down as they move downstream. In the axisymmetric model the vortices that form near the nozzle detach and move downstream without breaking down, thus causing fluctuations in radiation intensity to be overpredicted near the nozzle exit. In the Cartesian geometry calculations, large eddies develop near the nozzle exit (e.g., between 0 and 2 diameters downstream) that are not observed in the axisymmetric or three-dimensional calculations. A plausible explanation for their relatively large size compared with the other cases is due to the difference in how the area of the plume is computed in the different models. The three-dimensional model and the axisymmetric model use a physical area of πr^2, while the Cartesian case uses the length of a line segment. The longer path length through the eddies of the Cartesian geometry calculations causes the mean radiation intensity found using the time-dependent scalars to increase between the nozzle exit and 2 diameters downstream and then remain constant between 2 and 3 diameters downstream.

In both the axisymmetric and Cartesian coordinate calculations, the computed intensities decay more gradually downstream than in the measurements or three-dimensional calculations. In both cases entrainment and swirl in the in the third direction are not captured with the calculations. In the Cartesian case, the high-temperature region in the exhaust (e.g., 900 K) ends between 2 and 4 diameters downstream while the lower temperature region (e.g., 650 K) broadens downstream as a result of time-averaging of the large eddies that form in the flow. The plume width based on the temperature profiles is much wider than that which is indicated based by average measured intensity. The time-averaged scalar calculations in the three-dimensional calculations show the high-temperature region ending between 2 and 4 diameters downstream while the width of the lower-temperature region remains constant after an initial spreading between 0 and 2 diameters. In the axisymmetric case, limitations in entrainment and mixing are evident by the nearly uniform temperature profiles between 3 and 8 diameters downstream. An important limitation of axisymmetric detached eddy calculations (DES) is that the mixing across the centerline occurs only through molecular diffusion. The DES model reduces the turbulent viscosity in this region to values on the order of the molecular viscosity.

Acknowledgments

This work was supported by the U.S. Naval Surface Warfare Center, Crane Division. The aid of Brent Rankin and Benjamin Roberts is gratefully acknowledged for help in operating the combustor, acquiring and processing data, and calculating atmospheric attenuation. The nozzle was designed by Tony Tang. The aid of Michael Walls as technical supervisor is greatly appreciated.

References

[1] Bolkcom, C., Feickert, A., and Elias, B., "Homeland Security: Protecting Airliners from Terrorist Missiles," CRS Report for Congress, Rept. RL31741, 2005.

[2] Avital, G., Cohen, Y., Gamss, L., Kanelbaum, Y., Macales, J., Trieman, B., Yaniv, S., Lev, M., Stricker, J., and Sternlieb, A., "Experimental and Computational Study of Infrared Emission from Underexpanded Rocket Exhaust Plumes," *Journal of Thermophysics and Heat Transfer*, Vol. 15, No. 4, 2001, pp. 377–383. doi:10.2514/2.6629

[3] Heragu, S., Rao, K., and Raghunandan, B., "Prediction of Radiative Transfer from Potential Core of a Hot Jet," *Journal of Thermophysics and Heat Transfer*, Vol. 8, No. 2, 1994, pp. 368–370. doi:10.2514/3.548

[4] Mahulikar, S., Rao, G., Sane, S., and Marathe, A., "Aircraft Plume Infrared Signature in Nonafterburning Mode," *Journal of Thermophysics and Heat Transfer*, Vol. 19, No. 3, 2005, pp. 413–415. doi:10.2514/1.14686

[5] Chu, C.-W., Der, J., and Wun, W., "Simple Two-Dimensional-Nozzle Plume Model for Infrared Analysis," *Journal of Aircraft*, Vol. 18, No. 12, Dec. 1981, pp. 1038–1043. doi:10.2514/3.57597

[6] Decher, R., "Infrared Emissions from Turbofans with High Aspect Ratio Nozzles," *Journal of Aircraft*, Vol. 18, No. 12, 1981, pp. 1025–1031. doi:10.2514/3.44742

[7] Hewitt, C., and Black, W., "Effect of Line Doppler Shift on Plume Infrared Signatures," *Journal of Thermophysics and Heat Transfer*, Vol. 9, No. 4, 1995, pp. 636–643. doi:10.2514/3.718

[8] Blunck, D., and Gore, J., "A Study of Narrowband Radiation Intensity Measurements from Subsonic Exhaust Plumes," *Journal of Propulsion and Power*, Vol. 27, No. 1, 2011, pp. 227–235. doi:10.2514/1.47962

[9] Blunck, D., Harvazinski, M., Rankin, B., Merkle, C., and Gore, J., "Turbulent Radiation Intensity Statistics of Exhaust Plumes Exiting from a Subsonic Axisymmetric Nozzle," accepted for publication in *Journal of Thermophysics and Heat Transfer*, Vol. 26, No. 2, 2012, pp. 286–293.

[10] Knowles, K., and Saddington, A., "A Review of Jet Mixing Enhancement for Aircraft Propulsion Applications," *Journal of Aerospace Engineering*, Vol. 220, Part G, 2006, pp. 103–127.

[11] Dix, J., Saddington, A., Knowles, K., and Richardson, M., "Infra-Red Signature Reduction Study on a Small-Scale Jet Engine," *The Aeronautical Journal*, Vol. 109, No. 1092, 2005, pp. 83–88.

[12] Coelho, P., "Numerical Calculations of the Interaction between Turbulence and Radiation in Reactive Flows," *Progress in Energy and Combustion Science*, Vol. 33, 2007, pp. 311–383. doi:10.1016/j.pecs.2006.11.002

[13] Li, G., and Modest, M., "Importance of Turbulence-Radiation Interactions in Turbulence Diffusion Jet Flames," *Journal of Heat Transfer*, Vol. 125, 2003, pp. 831–838. doi:10.1115/1.1597621

[14] Viskanta, R., "Overview of Convection and Radiation in High Temperature Gas Flows," *International Journal of Engineering Science*, Vol. 36, 1998, pp. 1677–1699. doi:10.1016/S0020-7225(98)00053-6

[15] Faeth, G., Jeng, S., and Gore, J., "Radiation from Fires," *Heat Transfer in Fire and Combustion Systems*, Vol. 45, ASME HTD, New York, 1986, pp. 137–151.

[16] Kabashnikov, V., and Kmit, G., "Influence of Turbulent Fluctuations on Thermal Radiation," *Journal of Applied Spectroscopy*, Vol. 31, 1979, pp. 963–967. doi:10.1007/BF00614832

[17] Cox, G., "On Radiant Heat Transfer from Turbulent Flames," *Combustion Science and Technology*, Vol. 17, 1977, pp. 75–78. doi:10.1080/00102209708946815

[18] Jeng, S., Lai, M., and Faeth, G., "Nonluminous Radiation in Turbulent Buoyant Axisymmetric Flames," *Combustion Science and Technology*, Vol. 40, 1984, pp. 41–53. doi:10.1080/00102208408923797

[19] Gosman, A., and Ioannides, D., "Aspects of Computer Calculation of Liquid-Fueled Combustors," AIAA Paper 81-0323, 1981.

[20] Shuen, J.-S., Chen, L.-D., and Faeth, G., "Evaluation of Stochastic Model of Particle Dispersion in a Turbulent Round Jet," *American Institute of Chemical Engineers Journal*, Vol. 29, No. 1, 1983, pp. 167–170.

[21] Shuen, J.-S., Chen, L.-D., and Faeth, G., "Predictions of the Structure of Turbulent Particle-Laden, Round Jets," *AIAA Journal*, Vol. 21, 1983, pp. 1483–1484. doi:10.2514/3.8277

[22] Gore, J., Jeng, S., and Faeth, G., "Spectral and Total Radiation

Properties of Turbulent Carbon Monoxide/Air Diffusion Flames," *AIAA Journal*, Vol. 25, 1987, pp. 339–345.
doi:10.2514/3.9627

[23] Gore, J., Jeng, S., and Faeth, G., "Spectral and Total Radiation Properties of Turbulent Hydrogen/Air Diffusion Flames," *Journal of Heat Transfer*, Vol. 109, 1987, pp. 165–171.
doi:10.1115/1.3248038

[24] Zheng, Y., Sivathanu, Y., and Gore, J., "Measurements and Stochastic Time and Space Series Calculations of Spectral Radiation Intensities in a Turbulent Non-Premixed Flame," *Proceedings of the Combustion Institute*, Vol. 29, 2002, pp. 1957–1963.
doi:10.1016/S1540-7489(02)80238-3

[25] Zheng, Y., Barlow, R., and Gore, J., "Measurements and Calculations of Spectral Radiation Intensities for Turbulent Non-premixed and Partially Premixed Flames," *Journal of Heat Transfer*, Vol. 125, 2003, pp. 678–686.
doi:10.1115/1.1589502

[26] Pearce, B., and Varma, A., "Radiation–Turbulence Interaction in a Tactical Missile Exhaust Plume," AIAA Paper 81-1110, 1981.

[27] Gupta, A., Modest, M., and Haworth, D., "Large-Eddy Calculation of Turbulence-Radiation Interactions in a Turbulent Planar Channel Flow," *Journal of Heat Transfer*, Vol. 131, 2009.

[28] Mazumder, S., and Modest, M., "Turbulence-Radiation Interactions in Nonreactive Flow of Combustion Gases," *Journal of Heat Transfer*, Vol. 121, 1999, pp. 726–729.
doi:10.1115/1.2826041

[29] Wagner, W., and Pruss, A., "The IAPWS Formulation 1995 for the Thermodynamic Properties of Ordinary Water Substance for General and Scientific Use," *Journal of Physical and Chemical Reference Data*, Vol. 31, No. 2, 2002, pp. 387–535.
doi:10.1063/1.1461829

[30] Li, D., Sankaran, V., Lindau, J., and Merkle, C. L., "A Unified Computational Formulation for Multi-Component and Multi-Phase Flows," AIAA Paper 2005-1391, 2005.

[31] Venkateswaran, S., and Merkle, C. L., "Dual-Time Stepping and Preconditioning for Unsteady Computations," AIAA Paper 1995-0078, 1995.

[32] Travin, A., Shur, M., Strelets, M., and Spalart, P. R., "Physical and Numerical Upgrades in the Detached-Eddy Calculation of Complex Turbulent Flows," *412 EUROMECH Colloquium on LES of Complex Transitional and Turbulence Flows*, Munich, Oct. 2000.

[33] Menter, F. R., and Egorov, Y., "A Scale-Adaptive Calculation Model Using Two-Equation Models," AIAA Paper 2005-1095, 2005.

[34] Basu, D., Hamed, A., and Das, K., "DES, Hybrid RANS/LES and PANS Models for Unsteady Separated Turbulent Flow Calculations," , *Proceedings of FEDSM'05*, ASME FEDSM2005-77421, 2005.

[35] Baurle, R. A., Tam C.-J., Edwards, J. R., and Hassan, H. A., "Hybrid Calculation Approach for Cavity Flows: Blending, Algorithm, and Boundary Treatment Issues," *AIAA Journal*, Vol. 41, No. 8, 2003, pp. 1463–1480.
doi:10.2514/2.2129

[36] Wilcox, D. C., *Turbulence Modeling for CFD*, 2nd ed., DCW Industries, La Canada, CA, 1998.

[37] Modest, M., *Radiative Heat Transfer*, 2nd ed., Academic Press, New York, 2003, p. 271.

[38] Grosshandler, W., "RADCAL: A Narrow-Band Model for Radiation Calculations in a Combustion Environment," *NIST Technical Note 1402*, U.S. Government Printing Office, Washington, D. C., 1993, pp. 1–52.

[39] Pope, S., *Turbulent Flows*, Cambridge Univ. Press, New York/London/Cambridge, England, U.K., 2005.

[40] Kounalakis, M., Gore, J., and Faeth, G., "Turbulence/Radiation Interactions in Nonpremixed Hydrogen/Air Flames," *Proceedings of the Combustion Institute*, Vol. 22, 1988, pp. 1281–1290.

[41] Zheng, Y., Barlow, R., and Gore, J., "Spectral Radiation Properties of Partially Premixed Turbulent Flames," *Journal of Heat Transfer*, Vol. 125, 2003, pp. 1065–1073.
doi:10.1115/1.1621902